Water Absorption by Polymer Electrolytes Studied by NMR Imaging

Åsa Lauenstein and Jörgen Tegenfeldt*

The Ångström Laboratory, Inorganic Chemistry, Uppsala University, Box 538, SE−751 21 Uppsala, Sweden

Winfried Kuhn

International Imaging Corp., Langental 18, D-66440 Blieskastel, Germany

Received July 22, 1996; Revised Manuscript Received December 15, 1997

ABSTRACT: Water diffusion into the polymer electrolytes (Pb, Zn)$(CF_3SO_3)_2(PEO)_n$ leads to a dramatic increase of the ionic conductivity. Magnetic resonance imaging, MRI, has been used to study this water diffusion by one-dimensional mapping of properties such as spin density and relaxation times. The line widths are of a comparable magnitude for the polymer material and the absorbed water, which has been used to perform parallel studies of both components in the MRI experiments. The water absorption in the materials studied can be classified as Fickian diffusion. The effect of water ingress on crystallinity in semicrystalline samples with two-dimensional MRI has also been recorded. Water is absorbed mainly by the amorphous regions, although the diffusion of water through the sample is accompanied by a rapid destruction of the crystalline regions.

Introduction

The study of polymer electrolytes has been a popular subject in recent literature, where they have been suggested for applications such as thin-film batteries and ion-specific sensors.[1] The conductivity varies over a broad range, depending on the polymer matrix and concentration and type of salt, as well as temperature and morphology. An important group of polymer electrolytes is based on poly(ethylene oxide), PEO. Such materials have a large ability to absorb water from the surrounding air, with striking changes in ionic conductivity as a result. These changes can be explained in terms of polymer chain dynamics, ion−polymer interactions, and ion pairing. In a previous study, we used NMR spectroscopy to investigate the effect of water absorption on chain mobility of some PEO-based solid electrolytes, and we found an increasing mobility due to reduced crystallinity and to weaker cation-polymer interactions.[2] We have also studied the effect of water on self-diffusion of ions and polymer chain segments in short-chain systems, and we have related this to the modification of the ionic conductivity by hydration.[3] Little is known, however, about the absorption processes leading to these effects. To characterize the water ingress and its effects on structural and dynamic properties in polymer electrolytes, there is a need for spatially resolved information as a function of time.

Magnetic resonance imaging, MRI, is a branch of NMR spectroscopy and was first proposed by Lauterbur et al.[4] The technique has grown important in materials science over the last 10 or 15 years, since it provides spatial information about various properties; that is, one can produce a map showing the spatial distribution of NMR properties such as spin density, relaxation times, or diffusion constants in the sample.[5] MRI has proven to be particularly suitable for polymer materials,[6] and a number of studies have been performed on polymer−solvent systems. The most widespread application is to derive information about properties of the polymer matrix by recording a spin-density map of a solvent penetrating into it. Some examples are cross-linking density of polymers,[7−10] water distribution in composite materials,[11] and cavities in agar gels. In the latter case, the use of ^{17}O-enriched water makes it possible to study the signal from the penetrating solvent independently from that of the gel matrix.[12] Another approach is to describe the dynamic properties of the solvent, e.g., distribution of T_2 relaxation times,[13] diffusion coefficients,[14] or the effects of mixed-solvent systems.[15] Particularly interesting in the context of the present work are such studies of water in polycarbonates[16] and nylon.[17,18] Reports on the simultaneous NMR study of polymer matrix and solvent are, however, very rare; as far as we know, this was never reported for a water−polymer system, but there is such a study of deuterated hexane penetrating an elastomer.[19]

A widely used classification of solvent diffusion into polymers was first proposed by Alfrey et al.,[20] where case I and case II diffusions represent two opposite extremes. Case I diffusion obeys Fick's law, and commonly applies to amorphous polymers above T_g (rubbery state). The solvent diffusion is very slow compared to the polymer segmental relaxation rate, which results in an increase in solvent concentration from the polymer core to the swollen regions, while T_2 remains constant in the swollen region. Case I behavior in different polymer−solvent systems has been confirmed with MRI in, e.g., refs 13, 15, 17, and 18. In case II diffusion, wich commonly applies to amorphous polymers below T_g (glassy state), the solvent diffusion is much faster than the polymer segmental relaxation and characterized by a sharp boundary between the glassy core and the swollen polymer, advancing at a constant velocity. Here, the solvent concentration is constant throughout the swollen region, while the T_2 relaxation rate decreases toward the polymer core, as shown with MRI.[13,14] Exceptions from case I and case II behavior have been reported, e.g., due to phase transitions—other than from glassy to rubbery state—induced by the solvent ingress.[13] One example is the transition from crystalline to amorphous structure. The morphology in semicrys-

S0024-9297(96)01075-3 CCC: $15.00
Published on Web 05/23/1998

talline polymers has been studied following water absorption in nylon, where water is shown to enter the amorphous regions only.[17] Ercken et al.[13] report that ingress of acetone into polycarbonate induces crystallization.

With the present work, we have three principal goals. First, we want to examine the effects of water absorption on ionic conductivity in the polymer electrolytes $(Pb,Zn)(CF_3SO_3)_2(PEO)_n$. Second, we will use MRI to study the progress of water diffusion through the electrolytes, by one-dimensional mapping of properties such as spin density and relaxation time. Finally, the effect of water ingress on crystallinity in semicrystalline samples will be recorded with two-dimensional MRI. We will use the fact that the line widths are of a comparable magnitude for the polymer material and the absorbed water[2] to make parallel studies of both components in the MRI experiments.

Experimental Section

1. Sample Preparation. Polymer electrolytes based on PEO (BDH: MW = 4×10^6) were made using a two-solvent casting technique.[21] The preparation of $Zn(CF_3SO_3)_2$ (s) and $Pb(CF_3SO_3)_2$ (s) salts has been described elsewhere[2]. The resulting films were about 0.4 mm thick. For impedance measurements, the films were cast on plates of stainless steel to ensure good contact between the film and the electrodes. The polymer electrolytes used in the MRI measurements were cast on thin glass plates, resulting in adhesive films that easily stayed flat on the glass even when placed vertically in the sample tubes. Films of $M(CF_3SO_3)_2(PEO)_n$ were made for n = 9, 16, and 24, and for M = Pb and Zn. IR spectroscopy measurements proved that all components were dry before mixing, and the whole preparation took place in a glovebox (relative humidity <3%) at room temperature.

2. Ionic Conductivity Measurements. Before the electrical properties of the polymer electrolyte films were measured, the film samples were allowed to absorb water for 4 h in atmospheres of different relative humidity, each corresponding to a different water content in the sample. The samples were sandwiched between two thermostated parallel planar stainless steel electrodes. The latter were kept under a slight pressure by a spring-loaded holder to ensure a good contact between electrodes and electrolyte. The impedance measurements were performed at room temperature by ac impedance spectroscopy at frequencies ranging from 10 to 10^6 Hz, using a system based on a Solartron 1260 frequency response analyzer.

3. NMR Imaging Measurements. The proton NMR imaging measurements were performed on a Varian Unity-400 spectrometer equipped for microimaging at the Fraunhofer Institute for Biomedical Engineering in St. Ingbert, Germany. We used a home-built probe with a 10 mm solenoidal coil insert.

Two different setups were used to study the water ingress into the polymer films. In the first, shown in parts a and b of Figure 1, the polymer film was sandwiched between two thin glass plates and placed in a standard 10 mm NMR tube. Water was added at the bottom of the tube to produce a humid atmosphere. There was no direct contact between the polymer film and the water, but the polymer absorbed water only via the humid air. The glass plate−film package was wrapped in Teflon tape, so as to prevent water from getting in from more than one direction. The Teflon wrapping also helped keeping the sample hanging in the tube at a fixed distance from the water. This setup was used for the amorphous samples. One-dimensional profiles were recorded following the ingress of water into the film, to give spatially resolved information about changes in water content and dynamic properties of the water molecules and the polymer chains. In the second setup (Figure 1a,c), the film was attached only to a single glass plate, the one on which it was originally cast. Water could then be absorbed simultaneously by the whole film. This method was used for the partially crystalline samples. Two-dimensional T_2-weighted spin-density images were recorded during the water absorption to follow the changes in water content and morphology in the polymer film. For comparison, two-dimensional images were also recorded with the film covered as in the first setup, with water penetrating only from one edge.

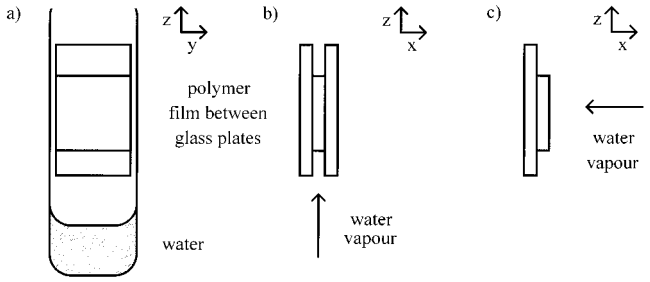

Figure 1. Experimental setup: (a) *yz* plane for 1- and 2-dimensional images; (b) *xz* plane for 1-dimensional images; (c) *xz* plane for 2-dimensional images.

The images were measured continuously during the water absorption. The measuring time for a two-dimensional image was 20 min. To increase the signal-to-noise ratio, T_1 and T_2 images were measured only as one-dimensional profiles. For comparison, one-dimensional spin-density profiles were also recorded. In this way, the time needed for each measurement was substantially decreased; a T_2 profile with 16 accumulated scans took about 15 min to record, and the corresponding spin density profile took only about a minute. This was considered to be relatively short in view of the diffusion rate of the water into the sample, and thus we did not expect any major artifacts due to water diffusion during the measurements.

One-dimensional profiles were recorded with a gradient strength of 23.4 G/cm along the sample tube axis (the Z axis in Figure 1), which resulted in a calculated pixel resolution of 40 μm along the profile. No slice selective gradient was applied, and consequently the resolution in the other two directions were equal to the film thickness and width, 400 μm and 9 mm, respectively. The actual resolution along the Z axis with respect to physical properties was within the range 50−200 μm, depending on the line width of the spectrum. Spin-density profiles were recorded using a Hahn spin−echo sequence[22] with a 90° pulse length of 3.5 μs. The time 2τ from the 90° pulse to the echo was 1.6 ms. For T_1 profiles, an aperiodic pulse saturating sequence was used for saturating the spins[23] followed by variable delays, τ, in a range between 10 ms and 3 s prior to the imaging measurement. T_2 profiles were measured using a Hahn spin−echo sequence where the echo time was varied between 1.0 and 10.5 ms. T_1 and T_2 data were then processed using the program Brainworks,[24,25] which resulted in spatially resolved representations of the T_1 and T_2 values.

Two-dimensional images were measured without slice selection, resulting in a calculated pixel resolution of 40 μm × 40 μm × 400 μm, where 400 μm was the thickness of the polymer film. The signal intensity within the images is displayed using a gray scale where white corresponds to zero signal. The time between the 90° pulse and the echo in the Hahn spin−echo sequence was 1.6 ms, the same as for the spin-density profiles. This excludes the spins with very short T_2 values in the relatively rigid polymer chains in dry and/or crystalline parts of the samples. However, as the polymer absorbs water, the line width decreases to about 2 kHz or less, which eventually allows a signal to be recorded. To ensure that the image was weighted by T_2 only and not by T_1, the time between scans was 5 s. The water signal was quite broad[2] and difficult to separate from the polymer signal. Therefore, we also used deuterated water to be able to study the proton signal from the polymer only.

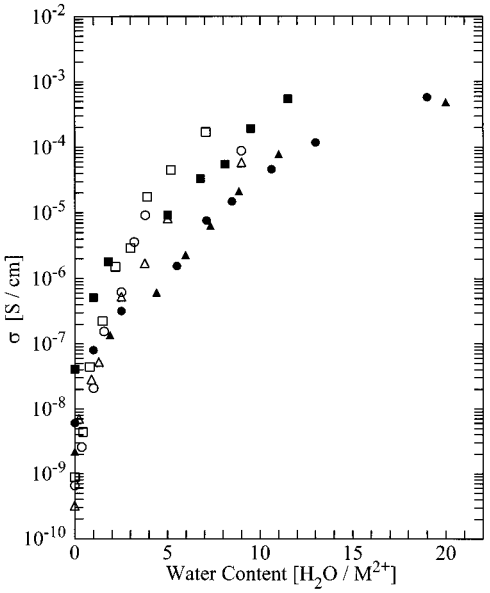

Figure 2. Ionic conductivity as a function of water content for $Pb(CF_3SO_3)_2(PEO)_n$ (open symbols) and $Zn(CF_3SO_3)_2(PEO)_n$ (filled symbols) with $n = 9$ (□), 16 (○), and 24 (△).

Results

1. Ionic Conductivity. The ionic conductivity as a function of water content was measured for the system $M(CF_3SO_3)_2(PEO)_n$ with M = Pb and Zn and $n = 9$, 16, and 24. The results are shown in Figure 2. All these electrolytes are hygroscopic and easily absorb water from the surrounding air, although the pure polymer absorbs water only at a humidity close to saturation.[2] Before each measurement, the polymer electrolyte film was allowed to take up water in an atmosphere with controlled humidity for at least 4 h, until no more water was absorbed. The water content in the samples was then determined by weighing, as described in ref 2. The zinc samples absorb more water than the lead samples at a given relative humidity.

The dry Zn samples show a higher conductivity than the dry Pb samples, almost by a factor of 50 for $n = 9$. There is also a concentration dependence. In dry $Pb(CF_3SO_3)_2(PEO)_n$, the conductivity for $n = 9$ is almost three times higher than for $n = 24$ and about 1.5 times higher than for $n = 16$, *i.e.*, the conductivity is roughly proportional to the salt concentration. In $Zn(CF_3SO_3)_2(PEO)_n$, the dependence on salt concentration is considerably larger: $n = 9$ produces a conductivity 18 times that for $n = 24$.

When the samples are allowed to take up water, the ionic conductivity increases for all compositions. $Pb(CF_3SO_3)_2(PEO)_9$ shows the fastest increase: when a sample absorbs four water molecules per cation, its conductivity increases by 4 orders of magnitude. Addition of the same amount of water to $Zn(CF_3SO_3)_2(PEO)_9$ causes an increase in conductivity by a factor of 200. Although the initial change is fast, the rate slows down for higher water contents. An increase from 4 to 12 water molecules per cation in $Zn(CF_3SO_3)_2(PEO)_9$ results in a conductivity increase by only a factor of 60. This, however, is primarily the case for M = Zn, and at a water content above four molecules per cation, the conductivity is higher at all concentrations for M = Pb than for M = Zn. The initial conductivity relation between the two ions is then reversed.

As the water content increases, the conductivity still shows a salt concentration dependence, although it is not as systematic as for the dry samples. The samples with $n = 9$ still show the highest conductivity. At five water molecules per cation, $Pb(CF_3SO_3)_2(PEO)_n$ with $n = 9$ shows five times higher conductivity than $n = 24$, while for $Zn(CF_3SO_3)_2(PEO)_n$ the factor is 15. At lower salt concentrations, however, the difference is very small, especially for M = Zn, where $n = 16$ and 24 exhibit roughly the same conductivity already at low water concentrations.

2. MRI on One-Dimensional Water Ingress in Amorphous Samples. Two-dimensional images in the YZ plane of $Zn(CF_3SO_3)_2(PEO)_9$ during absorption of deuterated water, D_2O, are shown in Figure 3. During the measurement, the film is sandwiched between two glass-plates and water is absorbed from the left in the picture. It was difficult to prevent absorption from the other edges, and some increase in signal is seen at top and bottom in the figure due to this unwanted absorption. Nevertheless, the one-dimensional traces shown above the images represent the middle region of the sample, relatively undisturbed by the unwanted absorption. All of the signal arises from the polymer protons, since D_2O is used. The one-dimensional traces show a sharp front progressing through the polymer, and the signal intensity is roughly constant within the interval studied. The front does not, however, proceed at a constant rate throughout the experiment, but its position is rather an approximately linear function of the square-root of time (Figure 4). In the $Pb(CF_3SO_3)_2(PEO)_9$ sample, the same time dependence is found. The front, however, is not as sharp as in the zinc case but shows an increase in signal intensity toward the edge of the film.

Images in the *YZ* plane recorded during absorption of normal protonated water, H_2O, in $Zn(CF_3SO_3)_2(PEO)_9$ are shown in Figure 5. The overall signal intensity is higher than in the D_2O case, as we now record the sum of the contributions from polymer and water. As before, the zinc sample exhibits a sharp diffusion front, while the signal intensity in the lead sample decreases toward the dry end of the film. A new, striking feature is the sharp peak arising from H_2O at the sample edge, where the polymer has contact with the humid air. This is seen for both zinc and lead. After 20 h, this peak has not changed its extension very much. Its intensity, on the other hand, increases continuously for at least 18 h. Additionally, the front progresses faster when H_2O is used. The difference is very large for the lead sample, where the signal is spread all over the sample (11 mm) after 24 h, whereas the front in the D_2O case has progressed only 2 mm during the same time. In the zinc sample, the D_2O behavior is approximately the same as for lead, while the H_2O front has moved about 3 mm.

3. Polymer Chain Dynamics During Water Ingress in Amorphous Samples. T_1 and T_2 relaxation data were recorded continuously during water uptake. The results for $Pb(CF_3SO_3)_2(PEO)_9$ are displayed in Figures 6 and 7. The figures show the T_1 and T_2 relaxation data calculated from the magnetization decay in each pixel along the *Z* axis in the regions of interest. The dry regions of the polymer, however, give no signal in the MRI experiments and are consequently not included in the figure. An overall feature to be noted for the experiments is the gradual change in T_1 and T_2 values over regions, both for lead and for zinc.

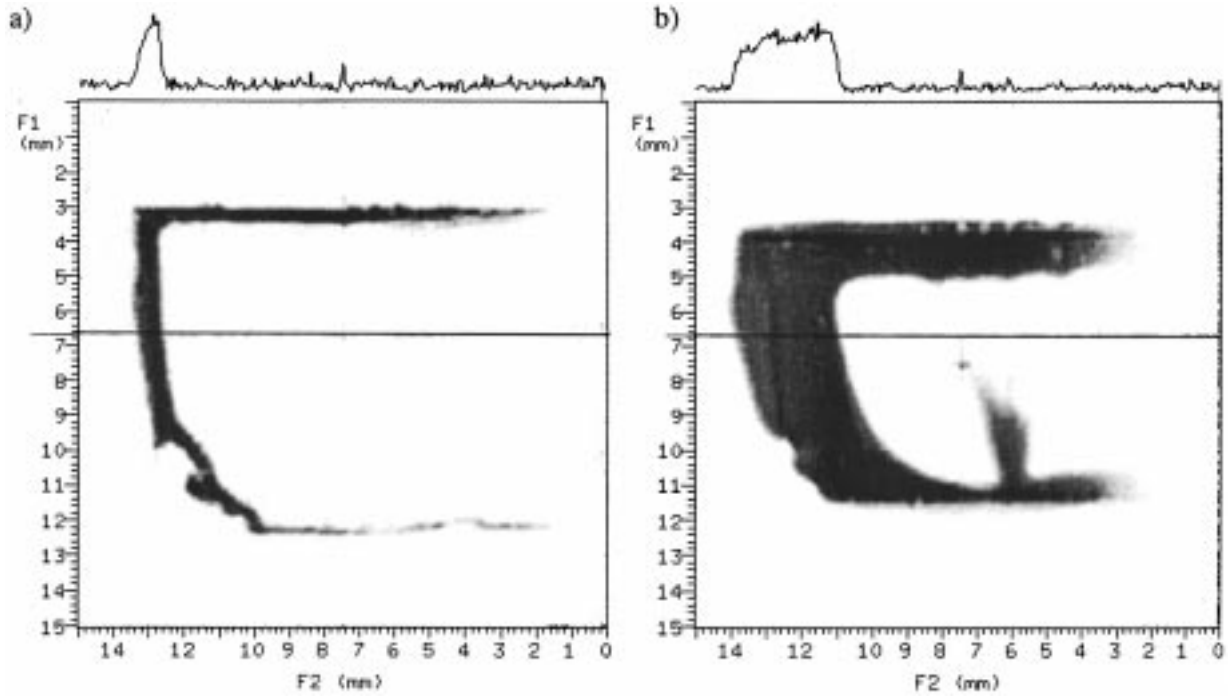

Figure 3. Proton spin density images and profiles for $Zn(CF_3SO_3)_2(PEO)_9$ during absorption of D_2O after (a) 2 h and (b) 21 h.

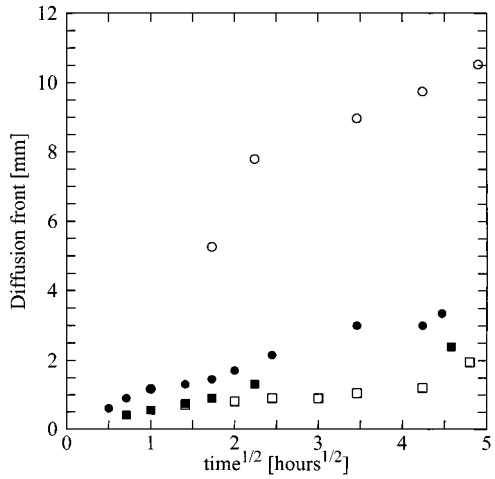

Figure 4. Progress of the diffusion front as a function of the square root of time for $Pb(CF_3SO_3)_2(PEO)_9$ with D_2O (□) and H_2O (○) and for $Zn(CF_3SO_3)_2(PEO)_9$ with D_2O (■) and H_2O (●).

Figure 6a shows the T_1 relaxation times in $Pb(CF_3SO_3)_2(PEO)_9$ as D_2O penetrates into the sample. In dry $Pb(CF_3SO_3)_2(PEO)_9$, T_1 is 1.45 s. After 1 h of exposure to D_2O, this value has decreased to 1.0 s at the diffusion front and 0.9 s at the film surface. The T_1 values decrease further as the absorption process goes on, and after 21 h, T_1 is 0.8 s at the front and 0.5 s at the surface. The effects of H_2O diffusion are shown in Figure 6b. The progress of the front is much faster than in the D_2O case, as seen from spin density images, and T_1 values measured at a given distance from the edge are lower than in the D_2O case. As water spreads in the sample, T_1 becomes constant over a broad range. After 21 h, T_1 is 0.6 s over a distance of almost 10 mm.

In the same manner, T_2 relaxation times were also measured during water absorption, and the results are shown in Figure 7a and 7b for $Pb(CF_3SO_3)_2(PEO)_9$ with D_2O and H_2O, respectively. T_2 in the polymer after 30 min of exposure is about 2 ms but increases on further water ingress. 21 h later, T_2 has increased to 10 ms at the film surface and to 3.5 ms 1.5 mm further in toward the diffusion front; thereafter, it stays roughly constant. Following absorption of H_2O, T_2 again increases to almost 10 ms at the surface after 21 h, although the increase is initially faster than for the polymer alone. The decrease in T_2 toward the constant region is faster and the constant value lower, 5.5 ms; it finally decreases again close to the diffusion front.

The T_1 relaxation time for dry $Zn(CF_3SO_3)_2(PEO)_9$ is 1.30 s. Following absorption of D_2O, the polymer T_1 values change in the same manner as in the lead case. At the film surface, T_1 has decreased to about 0.5 s after 1 h and stays constant, while at the diffusion front, it decreases from 0.75 s after 1 h of exposure to 0.6 s after 21 h. Yet, when H_2O is used, T_1 at the film surface initially decreases to 0.5 s but after 9 h it increases again. After 21 h, T_1 is 0.9 s. Meanwhile, T_1 at the diffusion front decreases from 0.5 to 0.4 s.

$Zn(CF_3SO_3)_2(PEO)_9$ does not exhibit any regions of constant T_2 relaxation times, but rather an overall increase with time. Each measurement shows a continuous decrease from the sample edge toward the diffusion front. The T_2 values are overall higher than in the lead sample. At the diffusion front, $Zn(CF_3SO_3)_2(PEO)_9$ shows a T_2 of 4−5 ms following absorption of D_2O and 8−9 ms for H_2O. At the sample edge, T_2 increases to well above 10 ms, which was the limit of our measurements due to the parameters chosen in the experiment.

4. Morphology in Crystalline Samples during Water Ingress. Two-dimensional images of $Zn(CF_3SO_3)_2(PEO)_{24}$ recorded during uptake of D_2O are shown in Figure 8. The film was cast on a glass plate and placed vertically in the NMR tube, where the entire film was exposed to a saturated D_2O atmosphere during the experiment, using the setup shown in Figure 1c. After 20 min of exposure, a signal appears, inhomogeneously distributed over the film (Figure 8a). Thirty minutes later, we can distinguish a pattern of white "spots" of 500−800 μm size, surrounded by darker regions (Figure

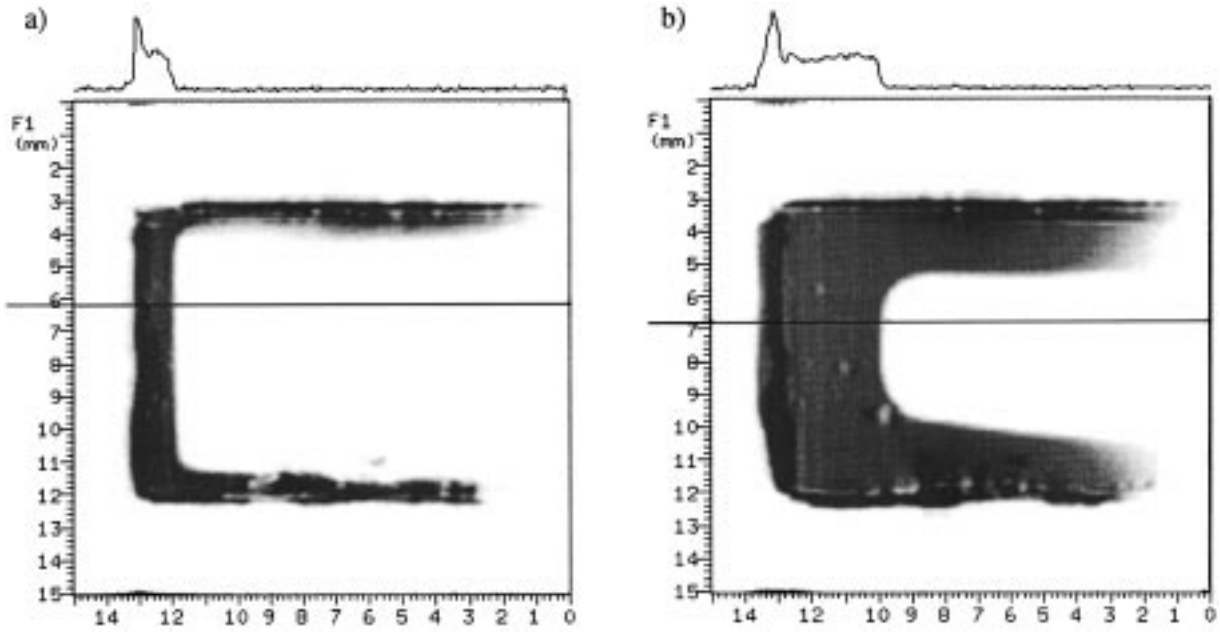

Figure 5. Proton spin density images and profiles for $Zn(CF_3SO_3)_2(PEO)_9$ during absorption of H_2O after (a) 2 h and (b) 20 h.

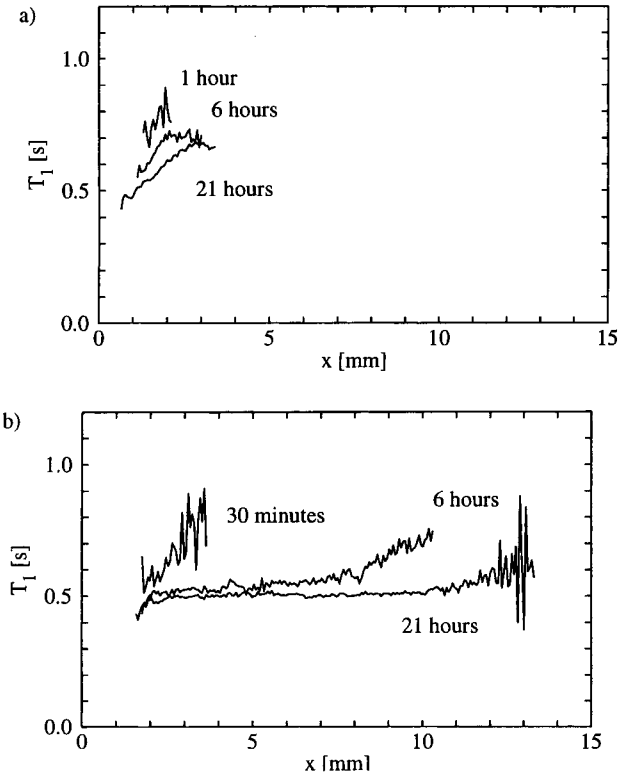

Figure 6. T_1 profiles for $Pb(CF_3SO_3)_2(PEO)_9$ during absorption of (a) D_2O and (b) H_2O.

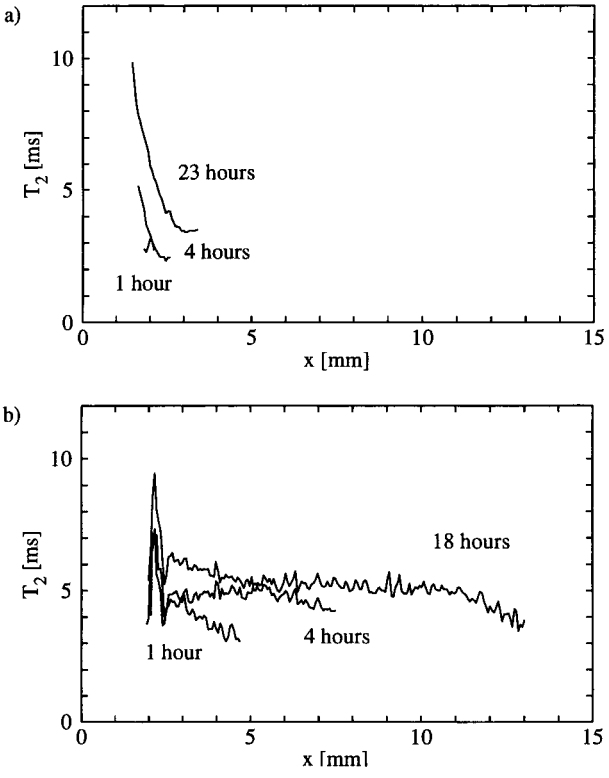

Figure 7. T_2 profiles for $Pb(CF_3SO_3)_2(PEO)_9$ during absorption of (a) D_2O and (b) H_2O.

8b). As shown by X-ray diffraction, $Zn(CF_3SO_3)_2(PEO)_{24}$ consists of microscopic regions of crystalline PEO and an amorphous PEO−salt complex, but it contains no crystalline complex.[26] Furthermore, a ^1H NMR spectrum shows one broad and one narrow component corresponding to crystalline and amorphous material, respectively.[27] In consistence with this, we find it reasonable to suggest that the MRI signal observed arises from amorphous material surrounding crystalline regions of 500−800 μm size. As the water absorption continues, the size of the crystalline regions decreases. Then, 100 min after the start of the experiment, a signal starts to grow also within the spots as the crystalline regions begin to dissolve, forming an amorphous phase (Figure 8c). Finally, after 4 h, no crystalline material is seen, but the image shows a homogeneous signal distribution throughout the sample (Figure 8d).

When a $Zn(CF_3SO_3)_2(PEO)_{24}$ film is allowed to absorb H_2O instead of D_2O, we see essentially the same pattern: white spots surrounded by regions with high signal intensity. The first signal is visible already after 10 min. Because of the added contribution from the water, the overall spin density signal increases faster than in the D_2O case. It is interesting to note that the

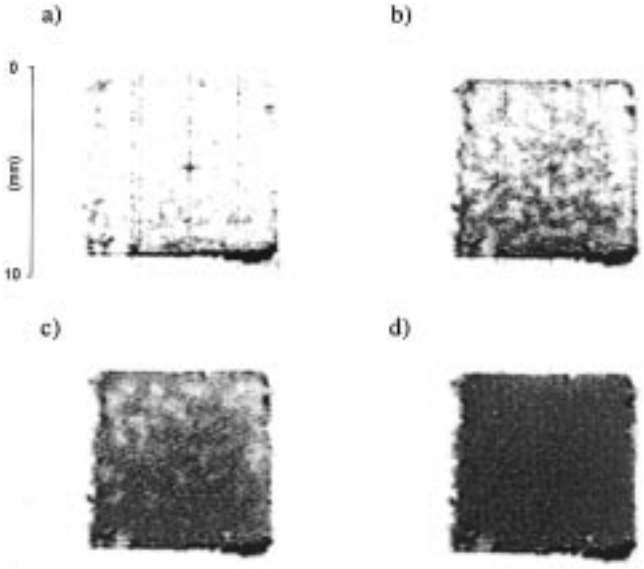

Figure 8. Two-dimensional spin density images of $Zn(CF_3SO_3)_2(PEO)_{24}$ during absorption of D_2O after (a) 20 min, (b) 50 min, (c) 100 min, (d) 4 h.

white regions are still of the same size, which indicates that water is not absorbed by the crystalline regions but only by the amorphous material. When the crystalline material dissolves to form an amorphous phase, however, the water content increases rapidly, and the whole image is soon homogeneously dark gray as a result of the increased signal intensity.

A $Zn(CF_3SO_3)_2(PEO)_{24}$ sample was also allowed to absorb H_2O from the edge, using the setup shown in Figure 1b. Two-dimensional images were recorded and are shown together with one-dimensional traces in Figure 9. After 1 h, we recognize the sharp diffusion front from the $Zn(CF_3SO_3)_2(PEO)_9$ experiment. As the experiment proceeds, water enters from more than one direction, which prevents further studies of the diffusion front from the one-dimensional traces. The two-dimensional images, however, show at least two remarkable differences compared to Figure 8. The first is the time-scale. Figure 8d shows a homogeneously wetted film after only 4 h of absorption, while the image in Figure 9b exhibits large differences in spin density between the edges and the center of the film still after 11 h of water absorption. (There are also some small inhomogeneities due to air bubbles in the film.) The other difference is the distribution of crystalline and amorphous regions. In Figure 9a, the water ingress proceeds with the same speed throughout the sample and shows no preference to certain regions. Thus, the transport of water through the polymer film is slow compared to the rate with which the crystalline regions are transformed to amorphous regions.

Discussion and Conclusions

1. Ionic conductivity. The ionic conductivity data presented in this work show a good agreement with a study published in ref 2, where we discussed several factors responsible for the rise in conductivity on water absorption: increase in the number of free ions; enhanced polymer chain mobility due to reduced energy barriers for changes in conformation; enhanced polymer chain mobility due to changes in the morphology of the polymer electrolyte; coordination of cations by water molecules causing weaker interactions between the polymer chain and the ions, which also increases the chain mobility but not necessarily the ionic conductivity.

The last one of these effects occurs only in the $Zn(CF_3SO_3)_2(PEO)_n$ system and could actually explain our present result, where the change in ionic conductivity is considerably larger for the $Pb(CF_3SO_3)_2(PEO)_n$ system than the $Zn(CF_3SO_3)_2(PEO)_n$ system when the same amount of water has been absorbed. The mobility of the Zn^{2+} ions with their weaker interactions to the polymer chain is not promoted by increased chain mobility to the same extent as that of the more tightly bound Pb^{2+} ions.

2. MRI on One-Dimensional Water Ingress in Amorphous Samples. Solvent ingress in polymer materials can often be classified according to the models introduced by Alfrey et al.,[20] as mentioned in the introductory section of this paper. Consequently, we will now examine our results from the $Pb(CF_3SO_3)_2(PEO)_n$ and $Zn(CF_3SO_3)_2(PEO)_n$ systems in order to attempt such a classification.

During D_2O ingress through $Zn(CF_3SO_3)_2(PEO)_9$, the spin density images show a sharp front progressing through the polymer, and the signal intensity is roughly constant from the edge of the film to the front. This would have been a clear indication for case II diffusion, provided the intensity had been proportional to the solvent concentration. However, the polymer signal intensity only reflects the fraction of polymer signal with a line width less than a threshold value, and as mentioned in the Experimental Section, the echo time used excludes any signal with a line width greater than 2 kHz. Thus, the signal is not directly a measure of the solvent concentration. Instead, the roughly constant signal intensity between the film edge and the front is, probably, only an indication that all of the polymer has reached sufficient mobility to contribute to the signal. The shape of the profile does not, therefore, give any indication of the diffusion type in this case. However, the rate of progress of the diffusion front provides a clue: the position of the front is proportional to the square-root of time, as expected for a Fickian diffusion (case I). Furthermore, the intensity profile using regular, protonated H_2O diffusing into $Zn(CF_3SO_3)_2(PEO)_9$ shows an additional feature compared to the D_2O case: starting from a high intensity at the edge of the film, the intensity drops rapidly and then levels off to a value staying roughly constant up to the relatively sharp diffusion front. In fact, the profile looks like a superposition of the polymer signal for the D_2O case and a decaying profile from H_2O carrying out Fickian diffusion. In the $Pb(CF_3SO_3)_2(PEO)_9$ sample, the same Fickian time-dependence of the front progress is found, but the front is not as sharp as in the zinc case.

Theory predicts that Fickian diffusion should be accompanied by a constant T_2 relaxation time for the solvent throughout the swollen region. Both $Zn(CF_3SO_3)_2(PEO)_9$ and $Pb(CF_3SO_3)_2(PEO)_9$ show a continuous increase in T_2 for the polymer induced by the water ingress. The water T_2, on the other hand, is roughly constant over a large part of the swollen region, except close to the edge and close to the front (Figure 7). In short, both the time-dependence of the diffusion front progress and the T_2 analysis imply a Fickian, or case I, diffusion mechanism in the systems studied.

A major difference between our present study and earlier investigations is the fact that the line width of the solvent signal is comparable to that of the polymer,

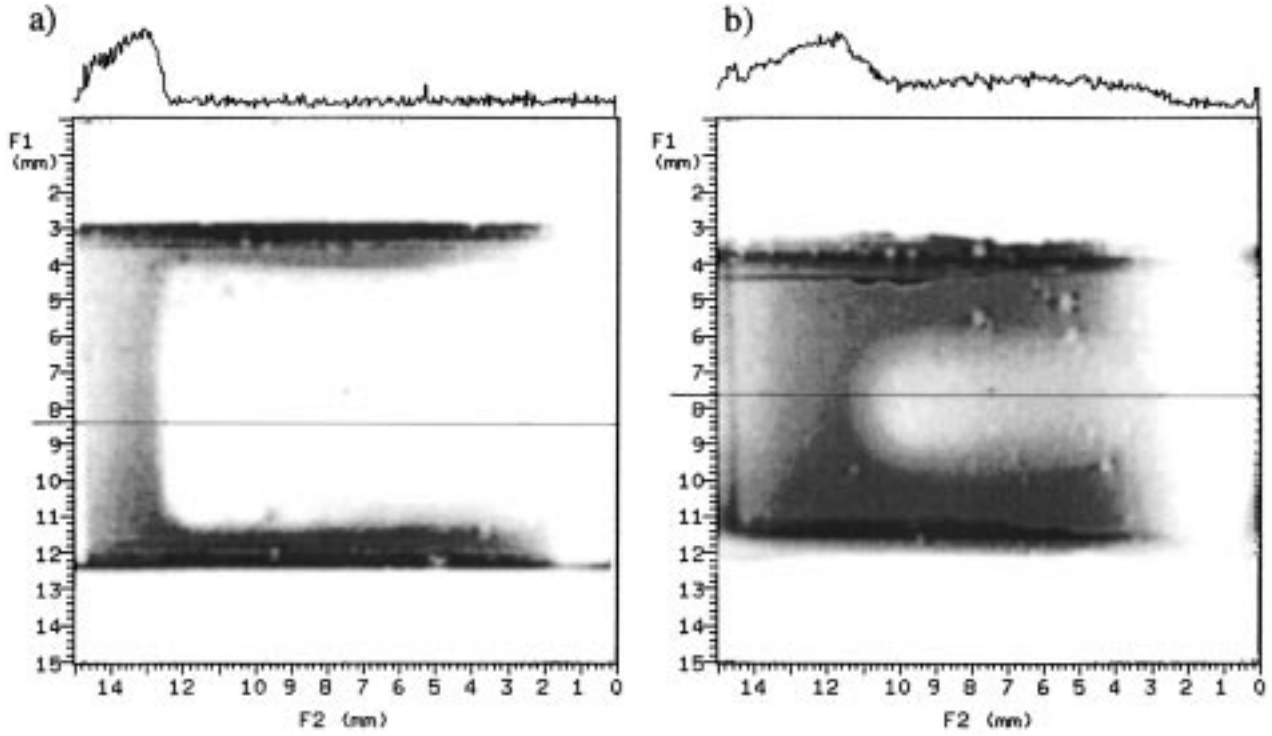

Figure 9. Proton spin density images and profiles for $Zn(CF_3SO_3)_2(PEO)_{24}$ during absorption of H_2O after (a) 1 h and (b) 11 h.

which makes it possible to study both components in the same experiment. As stated in the Experimental Section, the echo-time used excludes any signal with a line width broader than approximately 2 kHz. This results in images where the dry polymer with its line width of 30 kHz is invisible. Nevertheless, the decrease in line width on water uptake is a continuous process that starts immediately when the sample is exposed to humid air. We have earlier explained the increased mobility induced by hydration of these polymer electrolyte systems by the fact that the cations are coordinated by water molecules and do not cross-link the polymer chains.[2,3] Even small traces of water will affect the dynamic properties, indicated macroscopically by a decrease in the glass transition temperature and microscopically by a decrease of the line width of the proton NMR spectra. A spectrum of 2 kHz width arises from a $Pb(CF_3SO_3)_2(PEO)_9$ sample with more than three water molecules per lead ion.[2] This implies that the regions visible in the MRI experiment (with a line width less than 2 kHz) contain large amounts of water, while invisible regions still could contain quite substantial amounts. This is a possible explanation for the sudden "jump" in T_1 relaxation time from 1.45 in dry $Pb(CF_3SO_3)_2(PEO)_9$ to 1.0 s in the diffusion front, which, more specifically, represents the point where the line width of the polymer proton spectrum equals approximately 2 kHz and not the border between a wet and a dry region!

The situation for the water proton spectra is similar. Our earlier ^2H NMR study on deuterated water in $Pb(CF_3SO_3)_2(PEO)_9$ and $Zn(CF_3SO_3)_2(PEO)_9$ showed that no liquid water is present. This was concluded on the basis of the up to 20 kHz broad lines for water molecules in polymers with a low water content.[2] As a result, there could still be water present in regions of the sample that do not show in an MRI experiment, if the interactions with the polymer chain are strong enough to cause a line-broadening of the water signal. A comparison between the D_2O and H_2O experiments reported here also shows that the diffusion front progresses faster when H_2O is used. At a first glance, this would imply that some water could enter the sample without affecting the polymer dynamics. Using the same reasoning as above and again referring to ref 2, this is not the case. What these results, together with the relaxation time analysis, do tell us is that the dynamic properties of the water and the polymer differ, due to the very different molecular weight of the molecules – the water protons, as a rule, exhibit faster dynamics than the polymer protons at a given point in the sample—although they are strongly correlated. Bernson et al. have performed IR spectroscopy studies on polymer electrolyte systems and proposed several types of possible ion coordinations where hydrogen bondings of polymer OH groups play an important role as links between ions and polymer chains.[28,29] We find it probable that similar interactions exist with the OH groups of water molecules as links.[2]

The spin-density images recorded during H_2O uptake show that the water concentration is very high close to the sample edge compared to the rest of the sample. A water reservoir is formed in the interface between the film and the humid air. Armstrong and Clarke[30] suggested that the increased conductivity in polymer electrolytes on hydration should be due to salt dissolved in a water film adsorbed on the polymer surface. Still, the proton NMR spectra recorded together with our MRI measurements do not show any narrow components that could be assigned to liquid water. Additionally, we would expect liquid water to show different T_1 and T_2 relaxation characteristics than water bound to the polymer, but the spatial distribution of T_1 relaxation times following H_2O ingress in Figure 6b shows no drastic changes close to the edge. A comparison between Figure parts a and b of 7 indicates that the sudden changes in T_2 close to the sample edge on H_2O uptake arise from the polymer and not from the water.

On the contrary, the spatial dependence on water mobility is weak compared to that of the polymer. We conclude that the interactions between the water molecules and the polymer chain are strong enough to cause a line broadening of the water signal comparable to that of the polymer. Still, they allow the water molecules to move independently of the polymer chain as well as of the water concentration. The increased mobility of the polymer chain close to the sample edge is thus not due to weaker interactions with the water but rather to the larger freedom of the free ends in the plasticised wet regions compared to the chain segments close to the dry inner core of the film.

3. Morphology in Crystalline Samples during Water Ingress. The two-dimensional images of $Zn(CF_3SO_3)_2(PEO)_{24}$ absorbing D_2O show regions of 500−800 μm size with no observable spin density, surrounded by regions where polymer chains with a high mobility give rise to a large signal intensity. When H_2O is absorbed, the picture is still the same, although the signal intensity in the latter high mobility regions is considerably higher. We conclude that this increase is due to additional signal from water molecules and that water is absorbed mainly by the amorphous regions of the polymer, a common observation in semicrystalline polymers.[31]

In the semicrystalline polymer electrolytes studied here, one reason for the overall increase in polymer chain mobility on hydration is the reduced crystallinity, since the presence of crystalline regions restrict the mobility in the surrounding amorphous regions. The decrease in crystallinity has been probed by X-ray diffraction[21] and NMR spectroscopy.[2] Studies on poly(ethylene terephthalate), on the contrary, show that crystallization can be induced by swelling in methanol. Solvent ingress then increases the polymer chain mobility which promotes the reorientation required to form crystals, an effect similar to thermal treatment. Swelling agent expelled from the growing crystals accumulates on the surface of the spherulites so that the growth rate of the spherulites increases during crystallization.[32] In the $Zn(CF_3SO_3)_2(PEO)_{24}$ system studied here, however, the hydrated cation has an ability to coordinate a larger amount of PEO than the free ion, although the interactions are weaker.[2] This is a possible explanation for the increasing fraction of amorphous material: the coordination of polymer chains to the hydrated cations prevents crystallization. In Figure 8, we see how the size of the crystalline regions gradually decreases due to water uptake, and the boundary between amorphous and crystalline phase moves toward the core of the crystallites. Since the crystalline phase consists of pure PEO, the $Zn(CF_3SO_3)_2$ salt is distributed in the amorphous polymer−salt complex only. When the relative amount of amorphous phase increases, we expect a transport of ions toward the amorphous/crystalline boundary, where the polymer chain would prefer coordination to the hydrated cations rather than forming a crystalline structure. Figure 8d shows that this process is completed after about 4 h in D_2O atmosphere. In principle, it should be possible to follow the ion transport by ^{19}F imaging—this was not done in the present case, however.

The net migration of water through the film is considerably slower, as indicated in Figure 9, where large parts of the film are still unaffected by water absorption even after 11 h of exposure. Where water is absorbed, however, destruction of crystallinity and increase of chain mobility in the remaining amorphous phase occur almost instantly. In Figure 8, water was transferred only via the humid air, which limited the absorption rate. Here, on the other hand, we have a transport of water to the dry regions from a water reservoir, consisting of thoroughly swollen polymer chains, which provides an excess of water and speeds up the process. The faster kinetics appears to favor destruction of crystallinity rather than further progress of the water front through the amorphous regions. Decrease of crystallinity mainly involves a local reconstruction of the relatively weak polymer−polymer and polymer−ion bonds. A progress of the water front through the polymer, however, requires a net migration of water molecules which cannot occur without the breaking and forming of strong bonds between cations and water molecules, since a net migration of hydrated ions would create a gradient of either salt concentration (migration of cations and anions) or electric charge (only cations).

Summary

The ionic conductivity of the polymer electrolyte systems $Zn(CF_3SO_3)_2(PEO)_n$ and $Pb(CF_3SO_3)_2(PEO)_n$ increases by several orders of magnitude on hydration. This increase is mainly due to the creation of free ions and the increased chain mobility. The water absorption in the materials studied can be classified as Fickian diffusion. The dynamic properties of the absorbed water are coupled to those of the polymer chain, although there are differences due to the different size of the molecules. In a semicrystalline sample, water is absorbed mainly by the amorphous regions, although the diffusion of water through the sample is accompanied by a rapid destruction of the crystalline regions.

Acknowledgment. This work was supported by Vattenfall Utveckling AB, which is hereby gratefully acknowledged. Thanks are also due to Peter Barth at the Fraunhofer Institute of Biomedical Engineering for essential assistance with the MRI measurements.

References and Notes

(1) Armand, M. B.; Chabagno, J. M.; Duclot, M. J. In *Fast Ion Transport in Solids*; Vashita, P., Mundy, J. N., Shenoy, G. K., Eds.; North-Holland, New York, 1979; p 131.
(2) Lauenstein, Å.; Johansson, A.; Tegenfeldt, J. *J. Electrochem. Soc.* **1984**, *141*, 1819−23.
(3) Johansson, A.; Lauenstein, Å.; Tegenfeldt, J., *J. Phys. Chem.* **1995**, *99*, 6163−6.
(4) Lauterbur, P. *Nature* **1973**, *242*, 190−1.
(5) Kuhn, W. *Angew. Chem., Int. Ed. Engl.* **1990**, *29*, 1−19.
(6) Blümich, B. *Makromol. Chem.* **1993**, *194*, 2133−61.
(7) Kuhn, W.; Theis, I., Köller, E. *Mater. Res. Soc. Symp. Proc.* **1991**, *217*, 33−42.
(8) Kuhn, W.; Barth, P.; Hafner, S.; Simon, G.; Schneider, H. *Macromolecules* **1994**, *27*, 5773−9.
(9) Kuhn, W.; Barth, P.; Denner, P.; Müller, R. *Solid State NMR Spectrosc.*, in press.
(10) Kuhn, W.; Denner, P. *Macromolecules*, in press.
(11) Rothwell, W. P.; Holecek, D. R.; Kershaw, J. A. *J. Polym. Sci., Polym. Lett. Ed.* **1984**, *22*, 241−7.
(12) Mateescu, G. D.; Kinsey, R. A.; Yvars, G. M. *Mater. Res. Soc. Symp. Proc.* **1991**, *217*, 61−6.
(13) Ercken, M.; Adriaensens, P.; Vanderzande, D.; Gelan, J. *Macromolecules* **1995**, *28*, 8541−7.
(14) Weisenberger, L. A.; Koenig, J. L. *Macromolecules* **1990**, *23*, 2445−53.
(15) Webb, A. G.; Hall, L. D. *Polymer* **1991**, *32*, 2926−38.
(16) Fyfe, C. A.; Randall, L. H.; Burlinson, N. E. *Chem. Mater.* **1992**, *4*, 267−71.

(17) Mansfield, P.; Bowtell, R.; Blackband, S., *J. Magn. Res.* **1992**, *99*, 507−24.
(18) Fyfe, C. A.; Randall, L. H.; Burlinson, N. E., *J. Polymer Sci.: Part A: Polymer Chemistry* **1993**, *31*, 159−68.
(19) Rana, M. A.; Koenig, J. L.; *Macromolecules* **1994**, *27*, 3727−34.
(20) Alfrey, T.; Gurnee, E. F.; Lloyd, W. G.; *J. Polym. Sci.* (*C*) **1966,** *12*, 249−61.
(21) Wendsjö, Å.; Yang, H., *Proceedings of the 2nd International Symposium on Polymer Electrolytes*; Scrosati, B. Elsevier: Amsterdam, 1990; p 225.
(22) Hahn, E. L., *Phys. Rev.* **1950**, *80*, 580.
(23) Dietrich, W.; Bergmann, G.; Gerhards, R. *Z. Anal. Chem.* **1976**, *279*, 177.
(24) Brill, R., Staemmler, M. *A Framework Concept for Medical Work Station Design. Proceedings of the International Symposium of Computer Assisted Radiology (CAR) '*93 Berlin; Springer-Verlag: Berlin, 1993; p 775.
(25) Brill, R., Stahl, J., Staemmler, M., Gersonde, K. *SUNRISE II—A Versatile Environment for Medical Image and Data Processing. Tagungsband zum Workshop Visualiserung in der Medizin*, Medizin-Technische Transferstelle der Albert Ludwigs-Universität: Freiburg, Germany, 1993.
(26) Wendsjö, Å.; Lindgren, J.; Paluszkievicz, C.; *Electrochim. Acta* **1992**, *37*, 1689−93.
(27) Johansson, A.; Wendsjö, Å.; Tegenfeldt, J., *Electrochim. Acta* **1992**, *37*, 1487−9.
(28) Bernson, A.; Lindgren, J. *Polymer* **1994**, *35*, 4842−7.
(29) Bernson, A.; Lindgren, J. *Polymer* **1994**, *35*, 4848−51.
(30) Armstrong, R. D.; Clarke, M. D., *Solid State Ionics* **1984**, *11*, 305−6.
(31) Peterlin, A. *Pure Appl. Chem.* **1974**, *39*, 239−64.
(32) Zachmann, H. G.; Konrad, G. *Makromol. Chem.* **1968**, *118*, 189−210.

MA961075J